Moho Topography in the Central Andes from Teleseismic Receiver Functions and its Geodynamic Implications

Xiaohui Yuan, Stephan V. Sobolev and Rainer Kind (GeoForschungsZentrum Potsdam and Freie Universität Berlin)

Email: yuan@gfz-potsdam.de

SFB267

GEOFORSCHUNGSZENTRUM POTSDAM

More than 200 three-component seismic stations have been deployed in the central Andes from 1994 to 1997. We use P-to-S converted waves at the continental Moho together with multiple reflected waves between the Earth's surface and the Moho to estimate the Moho depth and crustal average V_P/V_S ratio. Our data confirm and significantly complement previous Moho depth estimates from wide-angle seismic studies (Wigger et al., 1994; Schmitz et al., 1999) and previous receiver function studies (Beck et al., 1996). The resulting crustal thickness varies from 35 km in the forarc area to up to 80 km beneath the plateau and it becomes thinner (30 km) further to the east in the Chaco Plain. Beneath the Andean plateau, the Moho is deeper in the north (Altiplano) and shallower in the south (Puna) where the plateau height is maximal. There is a non-linear correlation between crustal thickness and elevation which suggests that although most of the crust is felsic, the maficity of the lower crust gradually increase with depth. This correlation is also consistent with 80–100 km thick thermal lithosphere beneath Altiplano and by some 20 km thinner lithosphere beneath Puna. Non-increased thickness of the lithosphere in the regions of almost doubled crust strongly suggests that lithospheric delamination took place below the entire high-plateau. Relation between altitude and crustal thickness provides indication for thick lithosphere (up to 130–150 km) and lithospheric flexure below the Sub-Andean ranges at 19–20°S. The crust is thick (68 km) beneath the relative topographic low at the Salar de Atacama, which suggests that the lithosphere in this region is abnormally cold and is dynamically subsided. This may have a relation to the strongest (Ms=8.0) known intraslab earthquake in the Central Andes that happened very closely to this region in 1950. The average crustal V_P/V_S ratio is variable with highest values of 1.80–1.85 beneath the volcanic arc pointing to the high temperatures in the crust.

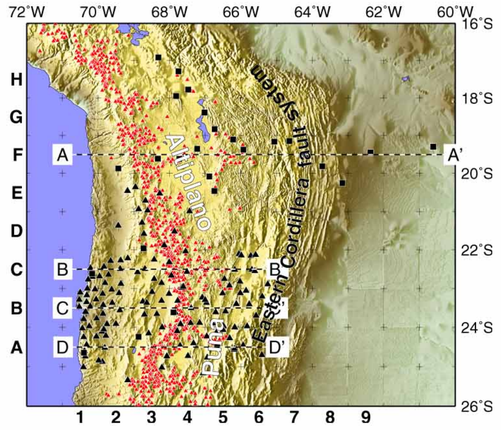

Figure 1: Topographic map of the Central Andes with major tectonic features indicated and seismic stations on it. Black squares are broadband stations (Guralp-3T and STS-2) operated for more than one year. Black triangles are short-period stations (Mark-L4) operated for two to three months. Volcanoes are marked with small red triangles. The entire area is subdevided into 1x1° boxes marked by croses, which are labelled in alphabetic and numerical orders shown at the left and bottom. Four east-west lines mark profiles shown in Fig. 2.

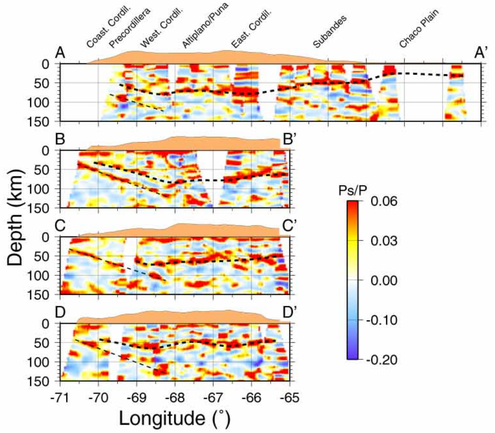

Figure 2: Four east-west depth receiver function profiles within latitude ranges of 1° each. The surface topography is averaged also within each latitude range. Positive receiver function amplitudes are shown in red while negative in blue. Dashed lines mark the continental and the subducted oceanic Mohos. Note that significant uplift of the Moho from the Altiplano (lines A–A' and B–B') to the Puna (lines C–C' and D–D') at 66–68°W, which is not accompanied by large altitude changes.

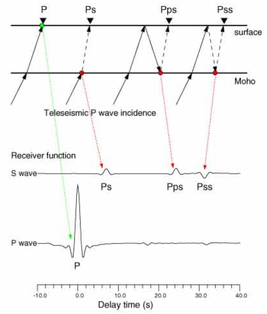

Figure 3: A teleseismic P wave propagating through the mantle and incident from below upon the crust and upper mantle beneath a seismic station will generate P-to-S converted waves (Ps) at any discontinuity beneath the station. Through reveicer function analysis, the converted waves can be isolated from the coda of the P wave, thus information on the velocity structure of the crust and upper mantle will be obtained. Usually strong energy of multiple reflected waves (mainly Pps and Pss) between the discontinuities and the Earth's surface are also contained in the receiver function data, providing an extra constraint on the depth estimate of the discontinuities and the average Vp/Vs ratio above the discontinuities.

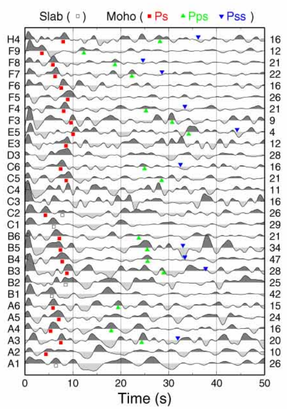

Figure 4: Summations of receiver functions for boxes shown in Fig. 1. The number of receiver functions stacked for each summation is plotted right to each trace. Directly converted phase and multiple phases are marked. Their times have been calculated with the models after the grid-search stacking.

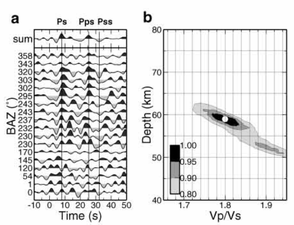

Figure 5: **(a)** Receiver functions of a broadband station within box B4 located in the volcanic arc are displayed equally spaced and sorted by back-azimuths, which are plotted to the left of each trace. Vertical straight lines mark directly converted phase and two multiple phases, labelled by Ps, Pps and Pss, respectively. **(b)** We use a grid-search algorithm (Zhu & Kanamori, 2000) by stacking the receiver functions at the times of the Ps and the multiple phases which are calculated for different Moho depths and crustal average V_P/V_S ratios. The best estimates of the Moho depth and the V_P/V_S ratio are found when the Ps and the multiple phases are stacked coherently (indicated by the white circle).

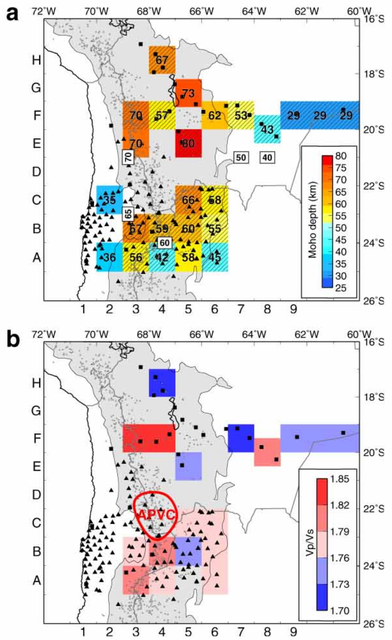

Figure 2: **(a)** Map of the Moho depth estimated. White boxes with numbers show depths to the Moho estimated from wide-angle reflection data (Wigger et al., 1994; Schmitz et al., 1999). We note the good consistency of the receiver function and wide-angle reflection results. **(b)** Estimates of the average Vp/Vs ratio in the crust. The highest Vp/Vs values are observed close to the volcanic arc. Data in the boxes D3, D4 and especially C3 and C4 (indicated by red countour) are strongly dominated by the negative conversions at middle crustal depths (Chmielovski et al., 1999; Yuan et al., 2000) which do not allow us to estimate reliably either the Moho depth or the average Vp/Vs ratio, but most likely indicate partially molten crust there.

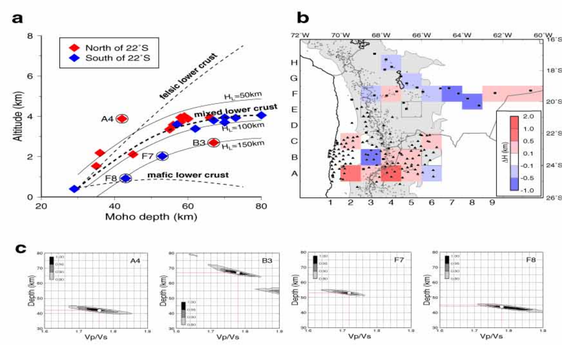

Yuan et al., Fig. 4

Figure 7: **(a)** Average altitudes versus depths to Moho in the 1x1° boxes. Blue diamonds correspond to the boxes north of the 22°S and red diamonds to the boxes south of the 22°S. Dashed lines show calculated isostatic altitude–Moho depth relations for the crusts composed from felsic rocks (upper curve), mafic rocks (lower curve) and mixed crust (middle curve). Curve shapes are mostly controlled by the crustal composition. Those curves are shifted parallel to the vertical (altitude) axis if thermal lithospheric thickness changes. Solid curves show expected altitude-Moho depth relations for the mixed felsic-mafic lower crust at 50, 100 and 150 km lithospheric thickness. Most of the data are consistent with mixed felsic-mafic composition of the lower crust and lithospheric thickness less than 100 km (fat dashed curve). However, there are four boxes with large deviation from the average curve. Corresponding points are outlined by the circles. **(b)** Difference between observed altitude and theoretically expected altitude (fat dashed curve in a). The largest negative deviations (blue – theoretical altitude too high) are located in Sub-Andean Ranges (F6 and F7) and in Salar da Atacama block (B3). Sub-Andean anomalies can be explained by about 50 km thickened lithosphere possibly in combination with lithospheric flexure. Salar da Atacama anomaly may be explained by cold lithosphere and dynamic subsidance due to the mechanical coupling of the cold lithosphere and subducting slab. This may have a relation to the strongest (Ms=8.0) known intraslab earthquake in the Central Andes that happened very closely to this region in 1950. Note that there is tendency for slightly too high elevation south of 21–22°S (rose-red colors) and slightly too low elevation north of 21–22°S (blue colors) which may be explained by about 20 km thinner, on average, lithosphere in the south. **(c)** Grid-search results for four regions which show the largest differences between observed and expected altitude showing high quality and reliability of these anomalous observations.

References:

(1) Beck et al., *Geology* **24**, 407–410, 1996.
(2) Chmielowski et al., *Geophys. Res. Lett.* **26**, 783–786, 1999.
(3) Wigger et al., in *Tectonics of the Southern Central Andes*, K. -J. Reutter, E. Scheuber and P. J. Wigger, Eds. (Springer Verlag, Berlin, 1994), pp. 23–48.
(4) Schmitz et al., *J. South. Am. Earth Sci.*, **12**, 237–260, 1999.
(5) Yuan et al., *Nature*, 2000 (in press).
(6) Zhu, L., and H. Kanamori, *J. Geophys. Res.* **105**, 2969–2980, 2000.